Title
Particle speciation of emissions from iso-butanol and ethanol blended gasoline in light-duty vehicles

Journal
Journal of Aerosol Science, 84

ISSN
00218502

Authors
Short, Daniel
Vu, Diep
Durbin, Thomas D
et al.

Publication Date
2015-06-01

DOI
10.1016/j.jaerosci.2015.02.010

Peer reviewed

Journal of Aerosol Science 84 (2015) 39–52

Contents lists available at ScienceDirect

Journal of Aerosol Science

journal homepage: www.elsevier.com/locate/jaerosci

Particle speciation of emissions from iso-butanol and ethanol blended gasoline in light-duty vehicles

Daniel Short [a,b], Diep Vu [a,b], Thomas D. Durbin [a,b], Georgios Karavalakis [a,b], Akua Asa-Awuku [a,b,*]

[a] Department of Chemical and Environmental Engineering, University of California – Riverside, Riverside, CA, USA
[b] College of Engineering – Center for Environmental Research and Technology, University of California – Riverside, Riverside, CA, USA

ARTICLE INFO

Article history:
Received 24 June 2014
Received in revised form
15 February 2015
Accepted 17 February 2015
Available online 5 March 2015

Keywords:
Particulate matter
Water-soluble organic carbon
Particle water-insolubility
Black carbon
Gasoline direct injection
Port fuel injection

ABSTRACT

Vehicular emissions of Particulate Matter (PM) will change under different driving conditions and as higher levels of alternative fuels are blended with gasoline. In particular, the chemical composition and water-soluble components of PM below 2.5 μm can be modified. In this study, three light-duty Port-Fuel Injection (PFI) and two Gasoline Direct Injection (GDI) vehicles were tested. All vehicles were tested over the Federal Test Procedure (FTP), Unified Cycle (UC), and at steady-state speeds (30, 50, and 70 mph) while operating on various ethanol and iso-butanol gasoline blends. The chemical and physical properties of the aerosol composition were measured via online/offline methods. Black carbon (BC), water-soluble organic carbon (WSOC), and droplet surface tension were measured. Water-Insoluble Mass (WIM) fractions were estimated from online size distribution measurements. Results show that the PFI vehicles, fuel composition and testing conditions (transient versus steady-state) impact PM emissions. GDI vehicles emit more PM and twice as much BC compared to PFI vehicles. Older PFI vehicles also produce more particles and BC emissions than newer vehicles. For three of the five vehicles, as speed increased, the WIM fraction increased. The results show vehicle operating conditions (steady-state or transient) can greatly impact the average composition of particles regardless of fuel composition.

1. Introduction

Port-Fuel Injection (PFI) vehicles have represented the vast majority of the U.S. Light-Duty Vehicle (LDV) market for several decades. Gasoline Direct Injection (GDI) vehicles have recently garnered attention due to their increased fuel economy and reduced carbon dioxide (CO_2) emissions. These vehicles are predicted to dominate the U.S. market in the next few years (Graham, 2005; Zhao e al., 2006). For PFI systems, the fuel is injected into the intake ports outside the combustion chamber during the intake stroke as the air moves into the combustion chamber. GDI engines, on the other hand, use an injection system similar to that used in diesel engines, but at a much lower pressure (Alkidas, 2007). For the GDI engines, the fuel is injected directly into the combustion chamber during the intake stroke, which provides higher thermodynamic efficiency and lower greenhouse gas emissions. The drawback is that the direct injection of fuel can lead to liquid fuel

* Corresponding Author.

http://dx.doi.org/10.1016/j.jaerosci.2015.02.010
0021-8502/

wetting on the piston bowl and cylinder surfaces and fuel-rich zones during combustion, which will likely result in higher emissions of particulate matter (PM) (Stevens & Steeper, 2001; Piock et al., 2011). A number of studies have shown that GDI vehicles produce higher PM and Particle Number (PN) emissions compared to their PFI counterparts (Liang et al., 2013; Aakko & Nylund, 2003; Ristimaki et al., 2005; Mamakos et al., 2013; Szybist et al., 2011; and references therein). PM can affect regional air quality, human health, and climate (IPCC, 2007; Nauss, 1995; Andreae & Rosenfeld (2008), Andreae & Crutzen, 1997; Baumer et al., 2008; Avol et al., 1979; Twomey, 1977; and references therein). Particles below 2.5 μm, ($PM_{2.5}$) can be inhaled deep within the lungs and can be deposited in the nose and subsequent access to the brain (Nauss, 1995; Yang et al., 2008; Oberdorster, 2001; Oberdorster et al., 2004). Long-term exposure to $PM_{2.5}$ has been linked to cardiovascular and pulmonary diseases (Pope et al., 2004; Mills et al., 2009). Hence, the number and size distributions of ultrafine particles from modern GDI and PFI vehicular emissions need to be characterized.

$PM_{2.5}$ that contains water-soluble material has the ability to form droplets. Particles that promote water vapor condensation and form droplets are termed Cloud Condensation Nuclei (CCN). By behaving as CCN, inhaled hygroscopic particles can grow to droplet sizes and enhance harmful PM deposition rates (Longest et al., 2010). In addition to affecting health, CCN emissions of water-soluble particles affect climate by altering cloud droplet formation and cloud properties (Ervens et al., 2005). Water-soluble PM can be toxic when inhaled (Ramgolam et al., 2009; Gutiérrez-Castillo et al., 2006; Valavandidis et al., 2008), and water-soluble particles have the ability to induce DNA damage (Gutiérrez-Castillo et al., 2006). Water-soluble matter can cause pro-inflammatory response, thus promoting pulmonary and cardiovascular diseases (Ramgolan et al., 2009). Furthermore, water-soluble and water-insoluble organic materials (WSOC and WIOC) and metals from vehicular emissions are highly correlated with the cellular production of reactive oxygenated species (ROS) linked to toxicity and detrimental health effects (Cheung et al., 2009; Geller et al., 2006; Verma et al., 2010; Biswas et al., 2009).

Limited studies have characterized the water-insoluble/soluble composition of gasoline vehicle emissions. Cheung et al. (2009) reported Water-Soluble Organic Carbon (WSOC) and Water-Insoluble Organic Carbon (WIOC) emissions from a PFI vehicle fueled with gasoline. The WSOC and WIOC were each found to compose ~20% of the total PM mass. Small amounts of elemental carbon (EC) were also emitted in their study (Cheung et al., 2009). To the best of our knowledge, little to no studies have characterized the water-insoluble/soluble composition from light-duty PFI and GDI vehicles with different alcohol fuel formulations. The addition of oxygenated fuels, such as ethanol and iso-butanol, can alter the resulting particle chemical composition and hygroscopicity. Thus, the potential influence of emissions of gasoline blends with different alcohols is not completely understood, especially with respect to regional air quality, health, and climate.

Black carbon (BC) is another important component of the vehicular PM composition. Black carbonaceous materials (i.e., soot or EC) are considered a significant source of insoluble material. Limited studies have investigated the contribution of BC to particle emissions from light-duty vehicles, especially as a function of different fuel compositions (Forestieri et al., 2013). Dutcher et al. (2011) found a decreasing trend of BC concentrations using an aetholometer with increasing ethanol content in gasoline in a PFI engine on an engine dynamometer. Giechaskiel et al. (2010) reported a ~90% increase in BC concentrations with increased vehicle speed from 50 to 140 km/h.

The objectives of this study are to evaluate the emissions of PFI and GDI vehicles over a range of ethanol and iso-butanol blends with an emphasis on characterizing particle hygroscopcity. Five vehicles were tested on seven fuels over the Federal Test Procedure (FTP), the Unified Cycle (UC), and at steady-state speeds of 30, 50, and 70 mph. This study investigates how factors, such as fuel type and driving cycle influence particle hygroscopicity, BC, WSOC, surface tension, and water-insoluble fractions.

2. Experimental

2.1. Test vehicles, fuels, and driving cycles

Three light-duty PFI vehicles and two GDI vehicles were tested for this study. The PFI vehicles tested were a 2007 Honda Civic (PFI 1), 2007 Dodge Ram (PFI 2), and 2012 Toyota Camry (PFI 3). The GDI vehicles tested include the 2012 Kia Optima (GDI 1) and 2012 Chevrolet Impala (GDI 2). Vehicle specifications can be found in Karavalakis et al. (2014).

A total of seven fuels were employed in this study, including ethanol and iso-butanol blends. Each vehicle was tested on E10 (10% ethanol and 90% gasoline), E15, and E20 blends. In addition to the ethanol blends, iso-butanol blends were used including B16 (16% iso-butanol and 84% gasoline), B24, and B32. The butanol blends of B16, B24, and B32 were the oxygenated equivalent of E10, E15, and E20, respectively. An alcohol mixture comprising of 10% ethanol and 8% iso-butanol (E10/B8) was also used in this study. It should be noted that only the PFI 3 and the GDI 1 were tested on the E10/B8 fuel blend. The fuels were custom made to maintain Reid Vapor Pressure (RVP), oxygen content, and fuel volatility and other properties. The main fuel properties can be found elsewhere (Karavalakis et al., 2014).

Each vehicle was tested on each fuel over three FTPs and three UC tests. The speed versus time plots for each cycle is shown in Fig. S1. The 6 tests on a particular fuel were conducted sequentially once the vehicle was changed to operate on that fuel, and the fuel was not changed to another fuel during this time. A fuel change with multiple drain and fills was conducted between the testing on each fuel to condition the vehicle and ensure no carryover effects. Detailed information on the driving cycles employed in this study and the testing protocol can be found elsewhere (Karavalakis et al., 2013). After transient operation, the vehicles were driven at steady-state speeds of 30, 50, and 70 mph for each fuel. Thus, the

steady-state emissions characterized the emissions from a "hot" catalyst. Due to operational constraints, not all fuels were tested at the steady-state speeds but all available data are presented.

The three steady-state speeds were driven for a duration of 30 min with 10 min for each steady state speed. The steady-state tests were performed after an FTP or UC test, which the three-way catalyst (TWC) and engine are both warm. Each vehicle was driven at 70 mph before the initial start of the test. The emission measurements would begin when the total particle concentration was steady without any large variation. The vehicles would be driven in the sequence of 70, 50, and 30 mph.

2.2. Emission testing and analysis

All tests were conducted in CE-CERT's Vehicle Emissions Research Laboratory (VERL), which is equipped with a Burke E. Porter 48-in. single-roll electric dynamometer. Gaseous and PM emissions were measured during each cycle and while the vehicle was operated at steady-state speeds. Fig. S2 shows the experimental set-up with flow rates of the various particle and gaseous instruments used for this study. A Pierburg AMA-4000 bench was used for gaseous emissions. Total particle number (PN) was measured with a TSI-3776 condensation particle counter (CPC) for the GDI vehicles and the PFI 1 and a TSI-3772 CPC for the PFI 1 and PFI 2. Results from both the PN and criteria pollutants from this study are provided in a separate journal article (Karavalakis et al., 2014).

BC concentrations were measured with a Multi-Angle Absorption Photometer (MAAP). The MAAP concentrates aerosol onto a Teflocarbon filter paper where a light with a 670 nm wavelength emits photons toward the aerosol concentrated area (Petzold & Schönlinner, 2004). The backscattering of photons was used to infer the mass of BC. This method determines the real-time concentration of BC from the emission stream for all particle diameters. The MAAP was calibrated using two different techniques. In the first technique, the temperature sensors and air flow rates were verified to be within 5% error of environmental conditions. For the second method, BC from a solutions of Aquadag© was aerosolized and the mass concentration was simultaneously measured with an Aerosol Particle Mass (APM, Kanomax Model 3600) Analyzer and the MAAP (Schwarz et al., 2006). The Aquadag calibration showed the MAAP measurements were within $\pm 11\%$ of APM measurements. BC emissions were reported by phase and for the overall UC and FTP.

Online particle hygroscopicity and Water-Insoluble Mass (WIM) fractions were estimated using a technique published in (Short et al., 2014). Briefly described here, the technique exploits discrepancies in particle size distributions measurements from a Water-based Condensation Particle Counter (W-CPC, TSI Model 3785) and Butanol-based CPC (B-CPC, TSI Model 3772). The two CPCs were connected in parallel with an electrostatic classifier (TSI Model 3080). The electrostatic classifier charges the particles with a Kyrpton-85 radiation source, size selects the dry polydisperse particle flow (particles that have not been exposed to the CPC working fluid) with a differential mobility analyzer (DMA, TSI Model 3081L) and generates a mono-disperse stream (Wang & Flagan, 1990). The monodisperse particles were then counted by both CPCs. Both CPCs produce their own particle size distributions which can be different due to the different working fluids (i.e., water and butanol).

The differences in the CPC particle counts below 250 nm are calculated by taking the ratio between the W-CPC to the B-CPC particle counts for each particle diameter selected by the SMPS. The assumption of this method is that all particles are counted in the B-CPC. The discrepancies between the two instruments, usually below 40 nm, are attributed to the particle hygroscopicity. These discrepancies are shown by calculating a hygroscopicity parameter named κ (Short et al., 2014). Unlike the study done previously in Short et al., 2014, only one SMPS is used which size selects the particle diameters then both the water and butanol CPCs count the particles from the one SMPS. However, the same calculations and theoretical assumptions can still be applied from Short et al., 2014. The determination of κ is described in Section 4. The term d_s, in the κ equation, is a particular particle diameter at which 50% of all particles were counted within the W-CPC. This was determined from the ratio of W-CPC to B-CPC particle counts for a given particle diameter. In this study, the Kelvin term, governed by the bulk fluid surface tension, was verified to have little to no effect on the water droplet activation properties. The experimental set-up was calibrated through the aerosolization of ammonium sulfate, with the method having a supersaturation of 2.3%. The corresponding theoretical equivalent diameter for activation, d_s, measured for ammonium sulfate was 20.5 nm, corresponds to a κ value that is equivalent to the known theoretical κ value for ammonium sulfate published in Petters and Kreidenweis (2007). The WIM fractions are calculated from the use of the κ value above in a two-component model that is explained in Section 2.5. The measurement of the κ value are valid at all ranges with this method, but the WIM fraction can only be inferred for values that are within the limits of the two-component model (Short et al., 2014).

The WIM fraction calculations were estimated for all three vehicles over the entire cycle and for each phase within the cycle. The overall cycle WIM fraction was calculated in a further step. Instead of comparing the CPC discrepancies from each 135 s SMPS scan, each diameter particle count was summed over the entire cycle. Thus, giving an overall cycle d_s to provide an overall cycle κ_{am}.

2.3. Emission factor

BC concentrations were reported in this study in units of $\mu g\,mi^{-1}$, or the Emission Factor (EF) of BC. The average BC concentration ($\mu g\,m^{-3}$), measured from the Constant Volume Sampler (CVS), was multiplied for each phase by the total volume of air through the CVS during each cycle phase (m^{-3}). The total BC mass for each phase is expressed in μg. The EF of

BC was calculated as follows:

$$\mathrm{EF(BC)} = 0.43\frac{\mathrm{BC}_1+\mathrm{BC}_2}{x_1+x_2}+0.57\frac{\mathrm{BC}_2+\mathrm{BC}_3}{x_2+x_3} \tag{1}$$

The numerator in these fractions includes terms for the total BC mass for each phase. For example, the total BC mass for phase 1 is BC_1. The denominator, x, is the total mileage traveled for each phase. For example, x_1, includes terms for the total mileage for the cold-start phase. The constant values 0.43 and 0.57 are weighing factors used to proportion the different phases of the cycle during vehicle certification.

2.4. Water-soluble organic carbon and surface tension measurements

Teflon filter samples were taken for each transient cycle test. Hence, the WSOC and surface tension measurements were representative of the cumulative aerosol composition over the FTP and UC. However, due to the accumulation of aerosols over the entire cycle it cannot determine the WSOC concentration for each phase. Filters were placed in vials and sonicated for 90 minutes with 60 mL of Millipore© DI water (18 mΩ, <100 ppb). Once sonicated, large non-dissolved particles were removed using a Whatman© 25 mm syringe filter. For the WSOC analysis, the sample was then diluted into ratios of 1:1, 1:3, and 1:5, with each vial containing 30 mL of sample. The surface tension, σ_b, for each sample was measured with a pendant drop tensiometer (Attension Theta 200). The tensiometer is an optical unit that uses the Young–Laplace equation to compute the droplet surface tension. For each droplet, 100 images were captured. The WSOC concentrations of these samples were measured using a GE Seivers 900 Total Organic Carbon (TOC) analyzer. Once the WSOC concentration was determined, the Water-Soluble Organic Mass (WSOM) can be found by multiplying the WSOC concentration by the volume of the initial water soluble and the constant 1.2. The constant 1.2 is an estimate of the average organic molecular weight per carbon weight (Turpin & Lim, 2001). WSOM was reported as an emission factor in units of mg/mi[1]. The WSOM emission factor was not calculated based on emissions per phase as in the BC emission factor. This emission factor was calculated using the filter loading parameters and divided by the total mileage for each cycle. The WSOM value was divided by the total PM mass to compute the WSOM fraction.

2.5. Water-insoluble mass fraction analysis

Rapid droplet growth in CPCs is possible when the saturation value, S, the ratio of the partial pressure (P_v) to the saturation pressure (P_{sat}) is greater than 1. Köhler's theory (Köhler, 1936) predicts the heterogeneous condensation of a bulk fluid vapor with a value S into the droplet S into the droplet phase (Eq. (2))

$$S = \frac{P_v}{P_{sat}(T)} = a_b\, exp\left(\frac{4M_b\sigma_b}{\rho_b RTD}\right) \tag{2}$$

where R is the universal gas constant, T is the temperature at activation, D is the wet droplet diameter, ρ_b is the density of the bulk fluid condensing onto the particle (water or butanol), M_b is the molecular weight of the bulk fluid, and σ_b is the surface tension at the droplet vapor/liquid interface, and a_b is the activity of solute in the bulk fluid. A critical supersaturation, s_c (equal to critical saturation, S_c-1), exists for which a minimum layer of condensed water on a particle is required to form a droplet. If the s_c becomes greater than 2% in the experimental setup; then uncontrollable particle growth will occur for particles above 40 nm (Seinfeld & Pandis, 2006). When σ_b is that of a ideal fluid, changes in particle activation for a given bulk fluid are controlled by the dissolved solute properties and the activity of the droplet solution.

The fluid activity, a_b, for the water droplet can be approximated by Raoult's Law. The rearrangement of Eq. (2) yields

$$\ln s_c = \left(\frac{4A^3}{27B}\right)^{1/2}, \quad A = \frac{4M_b\sigma_b}{\rho_b RT} \quad \text{and} \quad B = \frac{6n_sM_b}{\pi\rho_b} \tag{3}$$

where n_s is the moles of solute and ν is the ion dissociation of the particle in water (Seinfeld & Pandis, 2006). For a spherical solute particle, n_s is related to the dry particle diameter, d_s, the density of the particle, ρ_s and the molecular weight of the particle, M_s such that s_c and d_s are related as follows:

$$\ln {s_c}^2 = \frac{4A^3\rho_bM_s}{27\nu\rho_sM_b{d_s}^3} \tag{4}$$

At a given s_c, d_s is the theoretical critical diameter for activation, and the smallest diameter required for a fluid to condense on the particle surface (Seinfeld & Pandis 2006). The d_s value is obtained by finding the 50% efficiency of the ratio of W-CPC to B-CPC counts. It is an indication of the particle hygroscopicity that can be represented by a single solute parameter, κ (Petters & Kreidenweis, 2007). κ characterizes the effects of solute composition for droplet activation, and is calculated from fixed CPC s_c and from direct measurements of d_s giving Eq. (5)

$$\kappa = \frac{4A^3}{27{d_s}^3\ln(s_c)^2} \tag{5}$$

κ can range from 0 to 1, which 0 is water insoluble and 1 is very water-soluble. Eq. (5) is similar to Eq. (4) but Eq. (5) assumes the σ_b properties are that of a pure fluid. The κ value in Eq. (5) determines particle hygroscopicity. Assuming the particle is comprised of a completely water-soluble or water-insoluble compound, κ-hygroscopicity can be directly used to estimate a particles water-insoluble contribution (Petters & Kreidenweis, 2007). Water-insoluble composition changes can be approximated using a two-component model of a soluble and insoluble solute material. For our model, sulfuric acid (κ_{sa}=0.9) and dioctyl phthalate (κ_{DOP}=0.03) are used. Sulfuric acid has been measured in vehicular diesel exhaust and is believed to contribute to new particle formation through nucleation. Dioctyl phthalate (DOP) has been studied as a proxy for water-insoluble particle material from vehicular exhaust. With these model components, Eq. (6) estimates the water-insoluble mass fraction, χ

$$\kappa_{am} = \kappa_{sa}(1-\chi) + \kappa_{DOP}(\chi) \tag{6}$$

κ_{am} is the measured hygroscopicity of the unknown composition. The κ_{am} values assume a particle density of 1 $\mu g/m^3$. This method determines the WIM fractions for particle diameters below 40 nm. The WIM fractions are not valid for κ_{am} values that are above the κ_{sa} value or below the κ_{DOP} value. The WIM fractions are within 15% error uncertainty of actual WIM fractions (Short et al., 2014).

3. Results and discussion

3.1. Significant PN, PM mass, and particle size distribution vehicle trends

Results for measurements of the particle hygroscopicity and BC concentrations for each steady-state speed, the WIM fractions by each cycle phase and for the overall cycle, WSOM EFs and WSOM/PM Mass fractions, and BC EFs and BC/PM mass fractions are provided in this section. Karavalakis et al. (2014) reported additional information on the PM mass and PN emissions from these five vehicles previously. As this background information provides some basis for understanding the results in the current study, the PN and PM mass emissions in Karavalakis et al. (2014) are briefly summarized here. The PM mass emissions ranged from 0.1 to 1.45 mg/mi for the PFI vehicles and from 1.8 to 7.23 mg/mi for the GDI vehicles, while the PN emissions for the PFI vehicles ranged from 4.9×10^{10} /mi to 6.3×10^{11} /mi, and for the GDI vehicles ranged from 4.1×10^{12} /mi to 2.4×10^{13} /mi. Thus, the GDI vehicles had 5 times more PN and PM mass emissions compared to the PFI vehicles. Particle size distributions (PSDs) were measured for only the PFI vehicles in Karavalakis et al. (2013). The size distributions show that the majority of the particles are in the nucleation mode. Although PSDs were not measured for the GDI vehicles, Storey et al. (2010) have shown that the mode diameter is approximately ~50 nm, or in the accumulation mode size range under steady-state driving conditions.

3.2. Steady-state hygroscopicity and BC

The hygroscopicity estimates for sub-40 nm particles for all test vehicles during the steady-state conditions of 30, 50, and 70 mph are shown in Fig. 1. The data show that hygroscopicity increases with increasing vehicle speed. The higher κ_{am} is equivalent to lower amounts of water-insoluble PM. At 70 mph, all vehicles had the highest κ or hygroscopicity values. The GDI vehicles and the PFI 3 had κ_{am} values above 1.5 at 70 mph, which were higher than those for PFI 2 and PFI 1. It is important to note that most of the κ_{am} values at the 70 mph and 50 mph speeds for these fuels and vehicles are larger than the reported κ for sulfuric acid (i.e., $\kappa_{am} > 0.9$), a common soluble vehicular emission. Hence, using a simple two component model of sulfuric acid and DOP does not fully capture the WIM fraction of the aerosol. In fact, the estimated WIM fractions are actually negative, so these values are not shown. This indicates that the particles are very hygroscopic and can be considered fully wettable and water-soluble. It should be noted that $\kappa_{am} > 1$ corresponds to an activation diameter below 10 nm. Since particle sizes below 10 nm fall under from the lower detection limit of the SMPS, it is difficult to accurately characterize differences in κ_{am} values > 1. Particles at both 50 and 70 mph are likely both similar in nature to sulfuric acid or sulfate, which have κ_{am} values just below 1 and shouldn't be effect by the detection limits of the SMPS. Furthermore, surfactant effects (though negligible in the measured filters, which were not collected at steady-state speeds) could play a role at higher speeds. As these surfactants could be condensing onto the particle surface thus changing the perceived hygroscopicity. This is further described in Section 3.3. Most particle emissions at 30 mph were water-insoluble. At 30 mph, all five vehicles have κ_{am} values that are significantly lower than their respective 70 mph κ_{am} values. Decreasing vehicle speed decreased the hygroscopicity of PM from all tested vehicles.

BC concentrations are also shown to be higher with increased vehicle speeds for each of the test vehicles, as shown in Fig. 1. The GDI vehicles and the PFI 3 showed larger BC decreases with decreasing vehicle speed than PFI 2 and PFI 1. PFI 2 on the E10 fuel had a 16% decrease in BC concentration compared to a 93% decrease for PFI 3 between the 70 mph to 30 mph steady-state speeds. In addition, GDI 1 and GDI 2 had a 75% and 71% decrease, respectively, in BC concentration from the 70 mph to 30 mph speeds for the E10 fuel.

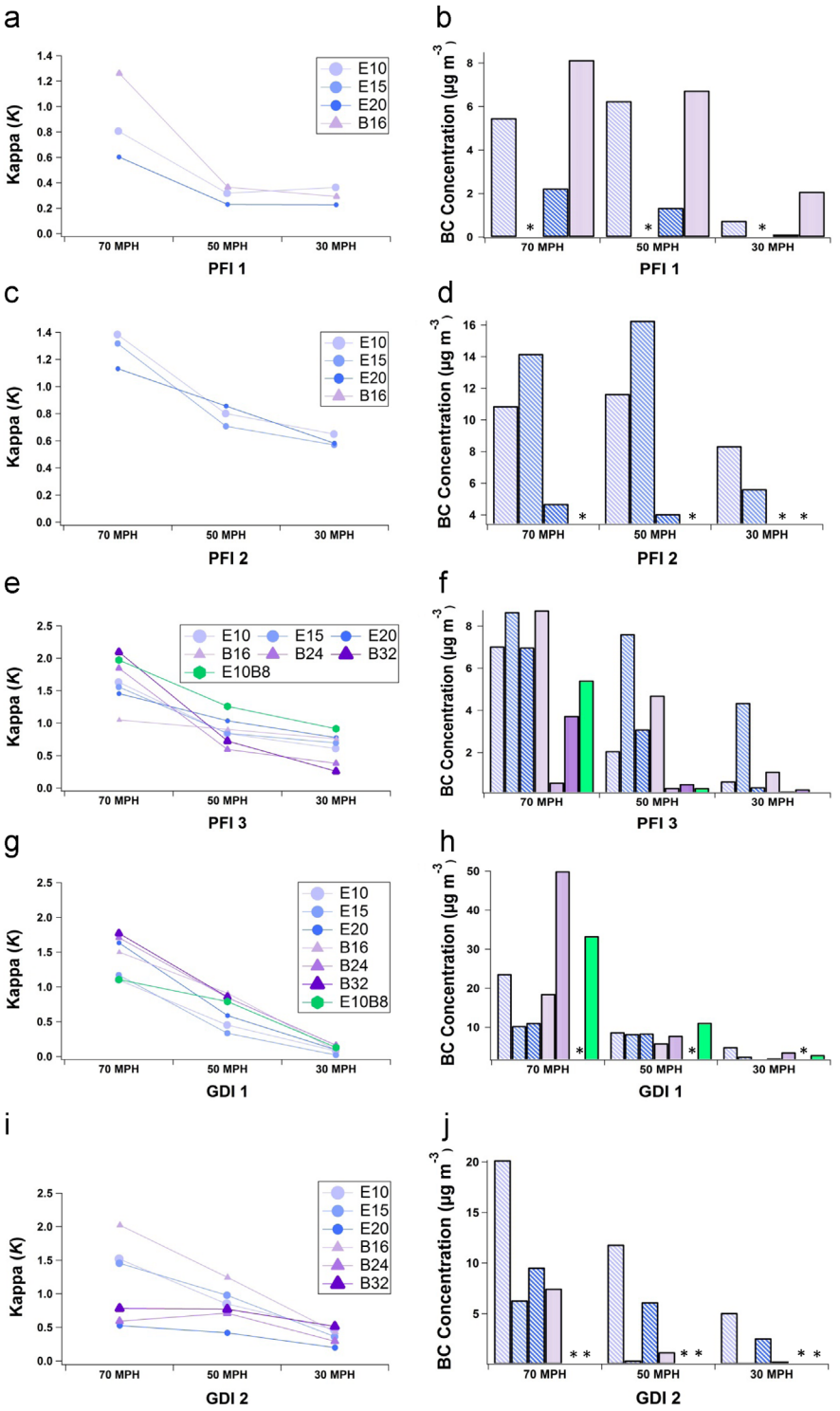

Fig. 1. The particle hygroscopicity parameter (κ) and BC concentrations for 3 steady-state speeds of 70, 50, and 30 mph for the PFI 1 {κ (a) and BC (b)}, PFI 2 {κ (c) and BC (d)}, PFI 3 {κ (e) and BC (f)}, GDI 1 {κ (g) and BC (h)}, and GDI 2 {κ (i) and BC (j)}. * Denotes data unavailable.

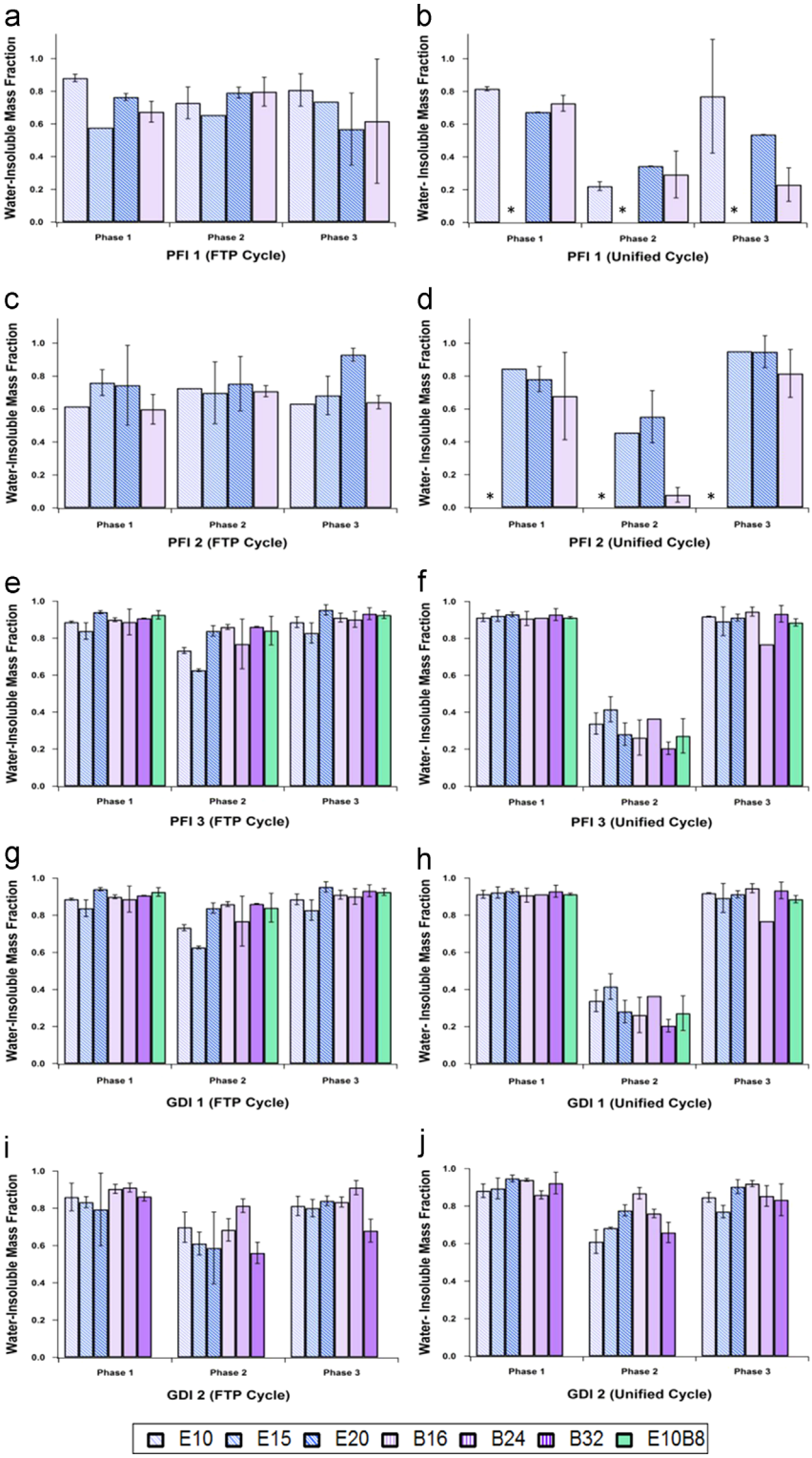

Fig. 2. Estimated water-insoluble mass fraction by phase of both the FTP and Unified Cycles for the PFI 1 {FTP (a) and Unified (b)}, PFI 2 {FTP (c) and Unified (d)}, PFI 3 {FTP (e) and Unified (f)}, GDI 1 {FTP (g) and Unified (h)}, and GDI 2 {FTP (i) and Unified (j)}. * Denotes data unavailable.

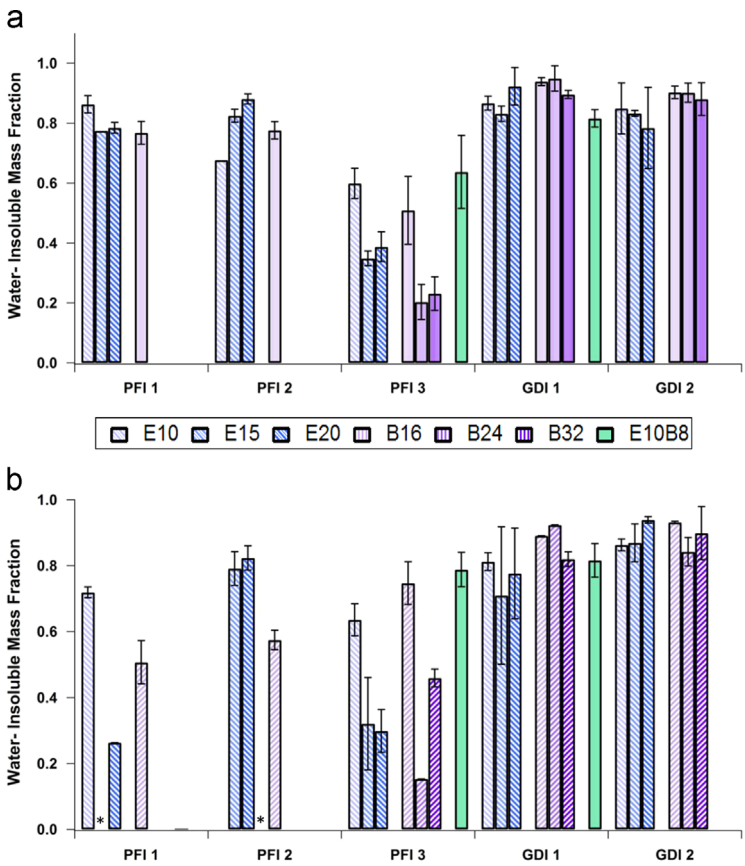

Fig. 3. Estimated water-insoluble mass fraction over the entire FTP (a) and UC Cycles (b) * Denotes data unavailable.

3.3. *Water-insoluble mass fraction*

Figs. 2 and 3 show the WIM fractions of each cycle phase and the cumulative WIM fractions, respectively, for all five vehicles. High WIM fractions indicate that particles emitted over the FTP cycle were mostly water-insoluble for all five vehicles. However, the UC shows different trends for the WIM fractions by phase. For the UC cold-start and hot-start phases for all vehicles, WIM emissions fractions remain similar to those for the FTP. PFI 1, PFI 2, and GDI 1, on the other hand, all show WIM fractions for the hot-running phase of the UC that decrease compared to the cold-start and hot-start phases. As higher vehicles speeds occur during the hot-running phase of the UC, these decreases were consistent with the results for the hygroscopicity measurements during steady-state conditions. In particular, driving conditions with the highest speeds (i.e., the hot-running phase of the UC) and the 70 mph steady-state speed show the lowest WIM fractions. The FTP cycle didn't see these significant changes with high speed due to the low high speeds (55 mph) in the cold-start and hot-start phases compared to the UC. A better understanding of particle solubility emission trends can be obtained by investigating the offline WSOM emission trends, as discussed below in Section 3.4. Over the FTP, PFI 3 exhibited lower WIM fractions compared to the other four vehicles. It should be noted that this vehicle, also had the lowest PM mass emission rates and the most prominent nucleation mode peak (Karavalakis et al., 2013).

The decrease in the WIM fraction between the cold-start and hot-running phases can be quantified for specific test fuels for different vehicles. When comparing the E10 fuel for the PFI 1 over the UC, a 70% decrease in the WIM fraction is shown from the cold-start to hot-running phase. For the E15 fuel on the PFI 2 over the UC, a 44% decrease of the WIM fraction was shown from the cold-start to hot-running phase. GDI 1 had the most consistent decrease in the WIM fraction over the UC for all fuels. For the E10 fuel, a 62% decrease in the WIM fraction was shown from the cold-start to hot-running phase over the UC.

Cumulative PM emissions, over both the FTP and UC, were mostly water-insoluble as shown in Fig. 3. Both GDI vehicles over the FTP cycle have cumulative WIM fractions of ~0.9. PFI 1 and PFI 2 also have cumulative WIM fractions over the FTP cycle of ~0.8. However, PFI 3 has lower cumulative WIM fractions compared to the other four vehicles. Similar trends were shown over the UC, even though a decrease in the WIM fraction is seen for phase 2 of the UC. This was due to the cumulative WIM fractions being dominated by the cold-start phase of the cycle, as a significant majority of the particles are emitted in the cold-start phase. For both cycles, lower vehicle speeds (i.e., speed below 55 mph) are found during the cold-start phase.

The cumulative WIM fractions show that the lower vehicle speeds during portions of the cycle where most of the particles are emitted produce higher water-insoluble particle emissions.

Fuel differences also changed the cumulative WIM fractions for some vehicles and fuels. PFI 3 was the only vehicle that had a consistent fuel trend over both cycles. Over the FTP cycle, PFI 3 showed a 53% decrease in the WIM fraction with increasing ethanol concentration from E10 to E20. PFI 3, with increasing ethanol and iso-butanol fuel concentrations over the UC, also showed decreasing WIM fractions of 53% and 40%, respectively. PFI 1 and PFI 2 both showed fuel effects over the UC. PFI 1 had a 61% decrease in the WIM fraction from the E10 to the E20 fuel on the UC. The E10/B8 fuel was comparable to both the E10 and B16 gasoline blends for PFI 3 and GDI 1, with a WIM fraction of 0.6. Comparing E10 to the B16 fuel blend over all five vehicles, B16 had a higher WIM fraction for PFI 3 and GDI 1. For both GDI vehicles, the WIM fractions were similar when comparing fuels over both cycles.

Potential correlations between the WIM fractions and fuel properties can be examined for the PFI 3, which showed the strongest fuel effects. Mono-aromatic compound concentrations decrease with increasing alcohol concentration for both the ethanol and iso-butanol fuel blends, as shown in Table 1. The WIM fraction for the PFI 3 also decreases with increasing alcohol concentration. Most mono-aromatic compounds (toluene, benzene, m-xylene, etc.) are considered to be water-insoluble. When plotting the mono-aromatic concentration against the WIM fraction, a R^2 value of 0.70 is shown. Although mono-aromatics may make up some of the water-insoluble particles below 40 nm measured in the cumulative WIM fractions for the PFI 3, other water-insoluble components (e.g., BC and inorganic material) could also contribute to the WIM fraction. Thus explaining the low R^2 value shown for the correlation. It should be noted that this correlation only works with the PFI 3 cumulative WIM fraction, as more sub-40 nm particles make up the total particle mass for this vehicle compared to the GDI vehicles. The GDI vehicles typically, on the other hand, have a particle mode diameter much larger at ~50 nm according to Storey et al., 2010, so the mode diameter is above the detection limit of the WIM fraction measurement.

Table 1
Table of mono-aromatic concentrations in fuels tested with the averaged cumulative WIM fractions over the FTP and UC for the PFI 3.

	E10	E15	E20	B16	B24	B32	E10/B8
Mono-aromatics (wt%)	26.23	20.91	18.31	25.47	20.69	19.80	26.75
FTP (WIM fractions)	0.5086	0.2310	0.2030	0.5990	0.3484	0.3875	0.6372
UC (WIM fractions)	0.7469	0.1531	0.4592	0.6353	0.3208	0.2987	0.7878

The correlation between high vehicle speeds and increasing particle water-solubility cannot be explained with certainty. However, one particular phenomenon could help determine the cause of the trend. A possible hypothesis is that some water-insoluble particles are being coated with a more water soluble layer. Cruz and Pandis (1998) verified the reverse case, that a coating of DOP around a water-soluble component, such as ammonium sulfate, decreased the activation diameter, d_s. thus, affecting measured particle hygroscopcity. Although DOP is very water-insoluble, it shows that it is possible to affect the perceived hygroscopicity of a particle by condensing different soluble material onto a particle. Our results may indicate that the condensing material is more soluble than the water-insoluble core. Iso-paraffin compounds have been shown to be able to break a part and oxidize (Yung-Fang, 1980; Curran et al., 2002). These oxidized compounds could be water-soluble and condense onto the particles emitted. The measured hygroscopicity of the particle is dictated by the composition on the surface of the particle rather than the particle core. Thus for our measurements, the composition of the particle surface decreased the actual particle hygroscopicity from highly water-insoluble to more water-soluble with increasing speed. Our results cannot definitively determine the composition of coatings that might be condensing on insoluble cores. Single particle chemical analysis was not collected here, but might provide additional information on possible soluble inorganic compounds. The bulk chemical composition information, on the other hand, provides little information about particle morphology.

3.4. Water-soluble organic mass emission factors and surface tension analysis

The WSOM EFs are shown for both the GDI 1 and GDI 2 over both cycles in Fig. 4 (a and b). In addition, the WSOM/PM mass fraction results are shown in Fig. 4 (c and d). These vehicles were selected for the WSOM analysis because they have the highest overall PM mass emissions. Note that the WSOM value is representative of the entire PM mass, whereas the WIM fractions in Section 3.3 only represent the mass of sub-40 nm particles. In addition, the WSOM EFs were calculated for the entire overall cycle and couldn't be determined for each phase in the cycle. The WSOM EF can be compared to the total PM mass to understand the amount of soluble organic mass emitted over each cycle. GDI 2 had much higher WSOM/PM mass fractions compared to the GDI 1. The WSOM/PM mass fractions for the FTP and UC ranged from 21% to 58%, respectively, for the GDI 2. GDI 1 shows fractions of ~20% of the total PM emissions for the FTP and UC.

Both the WSOM EFs and WSOM/PM mass fractions showed different fuel trends for both GDI vehicles. Generally, increasing iso-butanol concentration decreased the WSOM EF for both the vehicles and cycles, but the ethanol fuels did not show consistent trends. For GDI 1 and GDI 2 over the FTP cycle, a ~60% decrease in the WSOM emissions with increasing iso-butanol concentration was found, and for the GDI 1 over the UC, WSOM EF increased ~60% with increasing iso-butanol concentrations while the WSOM EF decreased ~40% over the same fuels over the UC for the GDI 2. GDI 2 also showed a

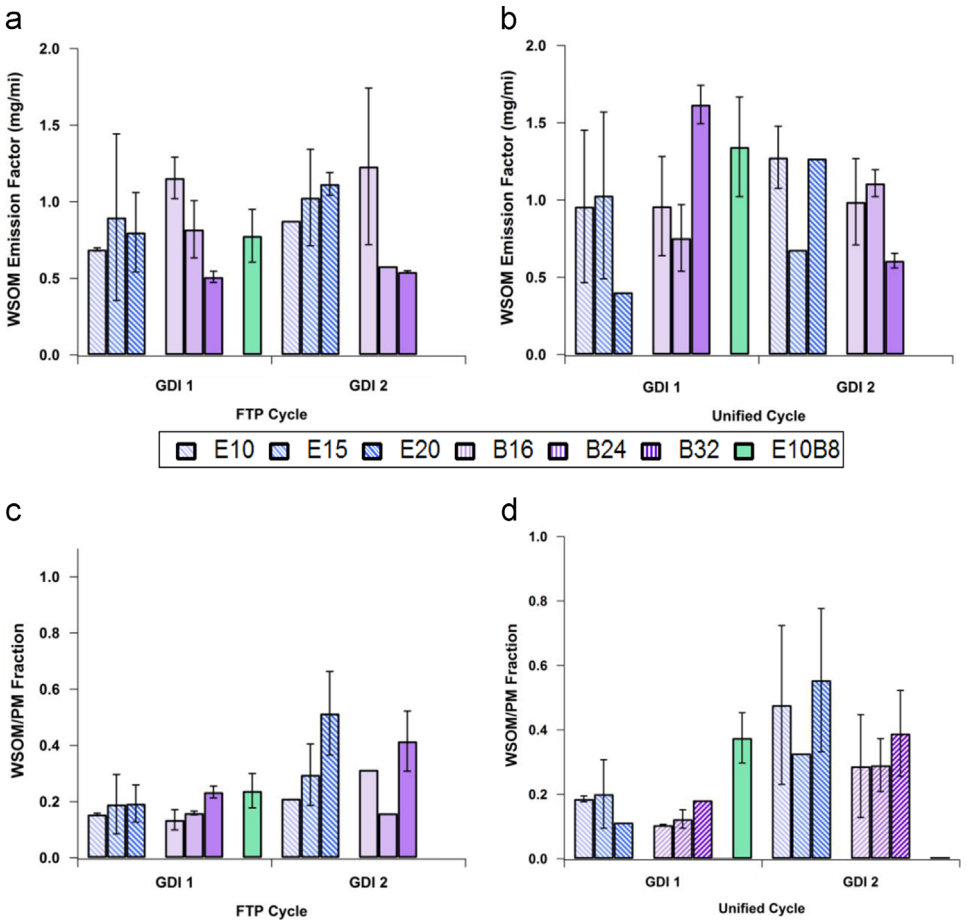

Fig. 4. The Water-Soluble Organic Mass (WSOM) emission factors over the FTP (a) and UC (b) and WSOM/PM fractions over the FTP (c) and UC (d) for both the GDI 1 and GDI 2.

~21% increase in the WSOM emissions with increasing ethanol concentration. The fuel trends were slightly different for the WSOM/PM mass fractions. GDI 2 showed different trends in the WSOM/ PM mass fractions, while the GDI 1 shows WSOM/ PM mass fractions there were consistently ~20% of the total PM emissions for the FTP and UC. For the GDI 2 over the FTP, the WSOM/PM mass fraction increased 180% from 20% to 55% with increasing ethanol concentration from the E10 to E20 fuel, while the iso-butanol fuel blends show a ~40% WSOM fraction with a slight increase with increasing alcohol content. These results were relatively consistent with WSOM measurements from a Euro 3 compliant Toyota Corolla tested in Cheung et al. (2009), where ~20% of PM emissions were found to be WSOM.

For GDI 2, the WSOM/PM mass results were not consistent with our WIM fractions measured in Sections 3.3, which showed relatively high levels of WIM. This lack of correlation is due to the PSDs. It is expected that the PSDs for the GDI 2 are similar to those from other GDI vehicles (Storey et al., 2010) and are dominated in the accumulation mode, which means most of the PN would be above the 40 nm threshold of the WIM fraction. Although particle below 40 nm may be predominately WIM, if the particle above 40 nm are more WSOM in nature than the PM mass as a whole would have a higher percentage of WSOM.

Surface tension was also measured for the same samples extracted for the WSOM analysis. The majority of these fuels and the vehicles emitted particles with a surface tension that closely resembles the surface tension of water. The surface tension of water at 23 °C and 1 atm is 72 mN/m. As a basis of comparison, the surface tension results are at a maximum with the E10 fuel on PFI 1 at 73.55 mN/m and are around 71 mN/m for PFI 3. GDI 1 and GDI 2 both have surface tension results on average of 72.95 ± 1.04 mN/m. As all the surface tension measurements are similar to the surface tension of water, this suggests that the assumption of pure water used in the κ calculation (Section 2.5) is valid.

3.5. *Black carbon emission factors*

BC also contributes to the particle mass. Figure 5 shows the BC EFs for the FTP and UC for all five vehicles. Unlike the WIM fractions that determined particle hygroscopicity for sub 40 nm particles, the BC EFs were determined for all particle

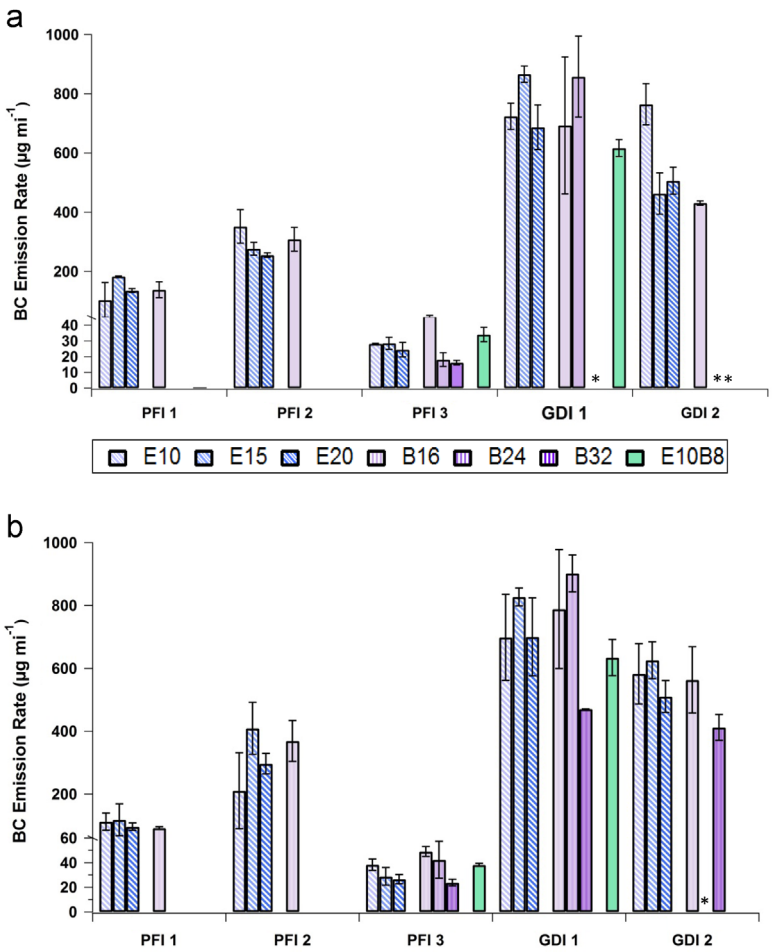

Fig. 5. Black Carbon emission factors over the entire (a) FTP and (b) UC cycles. * Denotes data unavailable.

diameters. Although BC is highly water-insoluble, it is hard to compare to the WIM fractions due to the method capturing only the particle insolubility below 40 nm. The BC EFs showed significant differences from vehicle to vehicle, but were similar for the FTP and UC for any given vehicle. The GDI vehicles had the highest BC EFs of all five vehicles over both cycles, and show about 5 times the amount of BC compared to the PFI vehicles. This is comparable to the differences in total PM mass and PN between the GDI and PFI vehicles, as discussed in Section 3.1. GDI 1 has slightly higher BC EFs overall ($\sim$800 µg mi^{-1}) compared to GDI 2 ($\sim$550 µg mi^{-1}) over the FTP cycle. Over the FTP cycle for the PFI vehicles, PFI 2 has the highest BC EF of the PFI vehicles over both cycles followed by PFI 1 and PFI 3, respectively. PFI 3 was the only vehicle that showed clear fuel trends over both cycles. Increasing ethanol and iso-butanol concentration over both cycles decreased BC EFs by 17% and 51%, respectively.

Fig. 6 shows the BC/PM mass fractions for the PFI 3, GDI 1, and GDI 2 for both the FTP and UC. Despite differences in the FTP and UC driving cycles, the testing regime did not affect the fraction of BC to PM emitted. For the majority of the vehicles, cycles, and fuels, the BC/PM mass fraction ranged from 0.1 to 0.3. Over the FTP cycle, all three vehicles show consistent BC/PM mass fractions at $\sim$0.20, with the exception of the PFI 3 showing a low BC/PM mass fraction of $\sim$0.05 for the iso-butanol fuels. For the UC, the GDI 1 BC/PM mass fractions remained at 0.20, similar to the FTP. GDI 2 showed a clear fuel trend over the UC of increased BC/PM mass fractions from 0.20 for the E10 fuel to 0.30 for the E20 fuel blend with a similar increase was also shown for the iso-butanol fuel blends. The PFI 3 showed BC/PM mass fractions of $\sim$0.02 to $\sim$0.13 over the UC, with lower mass fractions seen for the higher ethanol and iso-butanol blends.

The total PM mass is roughly 5 times the amount of BC emitted. It should be noted that the BC equivalent concentrations were based on optical methods from the MAAP. Other BC and soot-like measurements may use different wavelengths, measurement techniques, or may measure elemental carbon (EC) from filter media, as opposed to real-time methods (Slowik et al., 2007). In general, previous studies have shown that GDI PM is dominated by 80% to 90% soot/EC emissions (Maricq et al., 2013; Storey et al., 2014; Khalek et al., 2010; and references therein). Other BC measurement techniques (i.e., photoacoustic) have been shown to give a higher soot material mass compared to the MAAP (Slowik et al., 2007). Our measurements found BC or soot material to be lower at $\sim$20% (0.20 BC/PM mass fraction) of the total PM mass for GDI

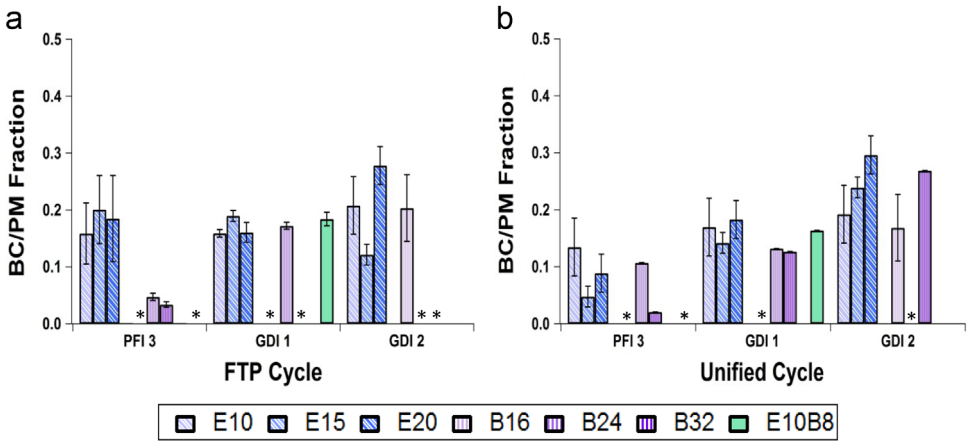

Fig. 6. BC PM fraction over the FTP (a) and UC (b) cycles * Denotes data unavailable.

vehicles, and suggest that further work on EC and BC methods of measurements is needed. For the PFI 3, assuming BC has similar properties to EC, the results were consistent with those from Cheung et al. (2009), where EC emissions represented a minor fraction of the total PM (roughly 5%).

The BC EFs showed similar trends to those of the WIM fractions. However, due to the WIM fractions being determined for fractions of the sub-40 nm it cannot be determined what composition is attributing to the particles being water-insoluble. The BC EFs represent all particle diameters not just the sub-40 nm region thus it cannot be said with the data shown in this study that BC is solely contributing to the WIM fractions. Other water-insoluble material may also have a significant contribution to the WIM fractions. In addition, the WSOM cannot correlate with the WIM fractions for similar reasons in that it is determined for all particle diameters not just the sub-40 nm region. The data presented in this study gives significant interest in the particle insolubility in the entire particle stream and also those in the ultrafine region that can be have human inhalation.

4. Conclusions

This study concluded that high steady-state speeds produce large fractions of sub-40 nm hygroscopic particles for both PFI and GDI vehicles. This was seen for both the higher steady-state speeds and for the higher speed and more aggressive phase 2 of the UC for the PFI 2, PFI 1, and GDI 1. As the steady-state speed decreases from 70 to 30 mph, the emitted particles become less hygroscopic and more water-insoluble for particle diameters below 40 nm. The particle emissions from the lower speed portions of the transient cycles were mostly non-hygroscopic and behaved like water-insoluble particles. The lower speed hot start phases and the hot running transient phase of the FTP all showed more water-insoluble particles. The cold-start phase, during of which the engine is cold and the TWC is below its light-off temperature, also produced non-hygroscopic particles. The enhancement of water-soluble particles has the ability to induce DNA damage, cause a pro-inflammatory response, and can promote pulmonary and cardiovascular disease (Ramgolan et al., 2009; Gutiérrez-Castillo et al., 2006). Thus, in addition to average daily driving emissions, the spatial regions in which high and low speed vehicle operation occurs must be studied; as the particle composition on high speed highways maybe significantly different than local residential driving. The difference in results could have important implications for ambient health studies. Future work to examine the correlation between the high vehicle speeds and low water-insoluble emitted particles is needed to determine the cause of these phenomena. However, this study provides evidence that particle composition changes occur with changing vehicle speed that should warrant further investigation.

Acknowledgements

The authors would like to thank Tyler Berte, Hans Phang, Chun Liang, and Wartini Ng for their contributions to this work. In addition, the authors thank Kurt Bumiller and Mark Villela for their technical support of the dynamometer test cell. This study was substantially supported by the California Energy Commission Grant number 500-09-051. Also, Daniel Short would like to acknowledge the funding support from the University of California Transportation Center (UCTC) Graduate Fellowship. Diep Vu thanks the U.S. Environmental Protection Agency (EPA) STAR Fellowship Assistance Agreement no. FP-91751101. Funding for BC measurements was made possible by the United States Environmental Protection Agency (EPA) Grant number 83504001. Its contents are solely the responsibility of the grantee and do not necessarily represent the official views of the EPA. Further, the EPA does not endorse the purchase of any commercial products or services mentioned in the publication.

Appendix A. Supporting information

Supplementary data associated with this article can be found in the online version at http://dx.doi.org/10.1016/j.jaerosci.2015.02.010.

References

Aakko, P. and Nylund, N.O. (2003). Particle emissions at moderate and cold temperatures using different fuels, SAE Technical Paper 2003-01-3285.

Alkidas, A.C. (2007). Combustion advancements in gasoline engines. *Energy Conversion and Management*, *48*, 2751–2761.

Andreae, M.O., & Crutzen, P.J. (1997). Atmospheric aerosols: biogeochemical sources and role in atmospheric chemistry. *Science*, *276*, 1052–1058.

Andreae, M.O., & Rosenfeld, D. (2008). Aerosol–cloud–precipitation interactions. Part 1. The nature and sources of cloud-active aerosols. *Earth Science Reviews*, *89*, 13–41.

Avol, E.L., Jones, M.P., Bailey, R.M., Chang, N.M.N., Kleinman, M.T., Linn, W.S., Bell, K.A., & Hackney, J.D. (1979). Controlled exposures of human volunteers to sulfate aerosols – health-effects and aerosol characterization. *American Review of Respiratory Disease*, *120*, 319–327.

Baumer, D., Vogel, B., Versick, S., Rinke, R., Mohler, O., & Schnaiter, M. (2008). *Relationship of visibility, aerosol optical thickness and aerosol size distribution in an ageing air mass over South-West Germany*. *Atmospheric Environment*, 42989–998 Sierra Research, Inc., Contract No. A932-185, Sacramento, California.

Biswas, S., Verma, V., Schauer, J.J., & Sioutas, C. (2009). Chemical speciation of pm emissions from heavy-duty diesel vehicles equipped with diesel particulate filter (DPF) and selective catalytic reduction (SCR) retrofits. *Atmospheric Environment*, *43*, 1917–1925.

Cheung, K.L., Polidori, A., Ntziachristos, L., Tzamkiozis, T., Samaras, Z., Cassee, F.R., Gerlofs, M., & Siouras, C. (2009). Chemical characteristics and oxidative potential of particulate matter emissions from gasoline, diesel, and biodiesel cars. *Environmental Science and Technology*, *43*, 6334–6340.

Curran, H.J., Gaffuri, P., Pitz, W.J., & Westbrook, C.K. (2002). A comprehensive modeling study of iso-octane oxidation. *Combustion and Flame*, *129*(3), 253–280.

Dutcher, D.D., Stolzenburg, M.R., Thompson, S.L., Madrano, J.M., Gross, D.S., Kittelson, D.B., & McMurry, P.H. (2011). Emissions from ethanol–gasoline blends: a single particle perspective. *Atmosphere*, *2*(2), 182–200.

Ervens, B., Feingold, G., & Kreidenweis, S.M. (2005). Influence of water-soluble organic carbon on cloud drop number concentration. *Journal of Geophysical Research*, *110*, D18211.

Forestieri, S.D., Collier, S., Kuwayama, T., Zhang, Q., Kleeman, M.J., & Cappa., C.D. (2013). Real-time black carbon emission factor measurements from light duty vehicles. *Environmental Science and Technology*, *47*, 13104–13112.

Geller, M.D., Ntziachristos, L., Mamakos, A., Samaras, Z., Schmitz, D.A., Fraines, J.R., & Sioutas, C. (2006). Physicochemical and redox characteristics of particulate matter (PM) emitted from gasoline and diesel passenger cars. *Atmospheric Environment*, *40*(36), 6988–7004.

Giechaskiel, B., Chirico, R., DeCarlo, P.F., Clairotte, M., Adam, T., Martini, G., Heringa, M.F., Richter, R., Prevot, A.S.H., Baltensperger, U., & Astorga, C. (2010). Evaluation of the particle measurement programme (PMP) protocol to remove the vehicles' exhaust aerosol volatile phase. *Science of the Total Environment*, *408*, 5106–5116.

Graham, L. (2005). Chemical characterization of emissions from advance technology light-duty vehicles. *Atmospheric Environment*, *39*(13), 2385–2398.

Gutiérrez-Castillo, M., Roubicek, D.A., Cebrián-Garcia, M.E., De Vizcaya-Ruiz, A., Sordo-Cedeòo, M., & Ostrosky-Wegman, P. (2006). Effect of chemical composition on the induction of DNA damage by urban airborne particulate matter. *Environmental and Molecular Mutagenesis*, *47*, 199–211.

IPCC (2007). Climate Change 2007: The Physical Science Basis. Summary for PolicyMakers.

Karavalakis, G., Short, D., Vu, D., Villela, M., Asa-Awuku, A., Durbin, T. (2013). Criteria emissions, particle number emissions, size distributions, and black carbon measurements from pfi gasoline vehicles fuelled with different ethanol and butanol blends, SAE Technical Paper, 2013-01-1147.

Karavalakis, G., Short, D., Vu, D., Villela, M., Asa-Awuku, A., & Durbin, T. (2014). Evaluating the regulated emissions, air toxics, ultrafine particles, and black carbon from SI-PFI and SI-DI vehicles operating on different ethanol and iso-butanol blends. *Fuel*, *128*, 410–421.

Khalek, I.A., Bougher, T., & Jetter, J.J. (2010). Particle emissions from a 2009 gasoline direct injection engine using different commercially available fuels. *SAE International Journal of Fuels Lubricants*, *3*(2), 623–637.

Köhler, H. (1936). The nucleus in and the growth of hygroscopic droplets. *Transactions of the Faraday Society*, *32*, 1152–1161.

Liang, B., Ge, Y., Tan, J., Han, X., Gao, L., Hao, L., Ye, W., & Dai, P. (2013). Comparison of PM emissions from a gasoline direct injected (GDI) vehicle and a port fuel injected (PFI) vehicles measured by electrical low pressure impactor (ELPI) with two fuels: gasoline and M15 methanol gasoline. *Journal of Aerosol Science*, *57*, 22–31.

Longest, P.W., McLeskey, J.T., & Hindle, M. (2010). Characterization of nanoaerosol size change during enhanced condensational growth. *Aerosol Science and Technology*, *44*(6), 473–483.

Mamakos, A., Martini, G., Marotta, A., & Manfredi, U. (2013). Assessment of different technical options in reducing particle emissions from gasoline direct injection vehicles. *Journal of Aerosol Science*, *63*, 115–125.

Maricq, M.M., Szente, J.J., Adams, J., Tennison, P., & Tumpsa, T. (2013). Influence of mileage accumulation on the paticle mass and number emissions of two gasoline direct injection vehicles. *Environmental Science and Technology*, *47*(20), 11890–11896, http://dx.doi.org/10.1021/es402686z.

Mills, N.L., Donaldson, K., Hadoke, P.W., Boon, N.A., MacNee, W., Cassee., F.R., Sandstom, T., Blomberg, A., & Newby, D.E. (2009). Adverse cardiovascular effects of air pollution. *Nature Clinical Practice Cardiovascular Medicine*, *6*(1), 36–44.

Nauss, K. (1995). *Diesel Exhaust: A Critical Analysis of Emissions, Exposure, and Health Effects*. Health Effects Institute: Cambridge, MA.

Oberdorster, G. (2001). Pulmonary effects of inhaled ultrafine particles. *International Archives of Occupational and Environmental Health*, *74*(1), 1–8.

Oberdorster, G., Sharp, Z., Atudorei, V., Elder, A., Gelein, R., Kreyling, W., & Cox, C. (2004). Translocation of inhaled ultrafine particles to the brain. *Inhalation Toxicology*, *16*, 437–445.

Petters, M.D., & Kreidenweis, S.M. (2007). A single parameter representation of hygroscopic growth and cloud condensation nucleus activity. *Atmospheric Chemistry and Physics*, *7*, 1961–1971.

Petzold, A., & Schönlinner, M. (2004). The multi-angle absorption photometer – a new method for the measurement of aerosol light absorption and atmospheric black carbon. *Journal of Aerosol Science*, *35*, 421–441.

Piock, W., Hoffmann, G., Berndorfer, A., Salemi, P., & Fusshoeller, B. (2011). Strategies towards meeting future particulate matter emission requirements in homogeneous gasoline direct injection engines. *SAE International Journal of Engines*, *4*, 1455–1468.

Pope, C.A., Burnett, R.T., Thuston, G.D., Thun, M.J., Calle, E.E., Krewski, D., & Godleski, J.J. (2004). Cardiovascular mortality and long-term exposure to particulate air pollution – epidemiological evidence of general pathophysiological pathways of disease. *Circulation*, *109*(1), 71–77.

Ramgolam, K., Favez, O., Cachier, H., Gaudichet, A., Marano, F., Martinon, L., & Baeza-Squiban, A. (2009). Size-partitioning of an urban aerosol to identify particle determinants involved in the proinflammatory response induced in airway epithelial cells. *Particle and Fibre Toxicology*, *2009*, 6–10.

Ristimaki, J., Keskinen, J., Virtanen, A., Maricq, M., & Aakko, P. (2005). Cold temperature PM emissions measurement: method evaluation and application to light duty vehicles. *Environmental Science Technology*, *39*, 9424–9430.

Schwarz, J.P., Gao, R.S., Fahey, D.W., Thomson, D.S., Watts, L.A., Wilson, J.C., Reeves, J.M., Darbeheshti, M., Baumgardner, D.G., Kok, G.L., Chung, S.H., Schulz, M., Hendricks, J., Lauer, A., Kärcher, B., Slowik, J.G., Rosenlof, K.H., Thompson, T.L., Langford, A.O., Loewenstein, M., & Aikin, K.C. (2006). Single-particle measurements of midlatitude black carbon and light-scattering aerosols from the boundary layer to the lower stratosphere. *Journal of Geophysical Research*, *111*, D16207.

Seinfeld, J.H., & Pandis, S.N. (2006). *Atmospheric Chemistry and Physics: From Air Pollution to Climate Change*. John Wiley & Sons, Inc.: Hoboken, New Jersey.

Short, D., Giordano, M., Zhu, Y., Fine, P., Polidori, A., & Asa-Awuku, A. (2014). A unique on-line method to infer black carbon contributions to water-insoluble contributions. *Aerosol Science and Technology*, *48*(7), 706–714.
Slowik, J.G., Cross, E.S., Han, J.-H., Davidovits, P., Onasch, T.B., Jayne, J.T., Williams, L.R., Canagaratna, M.R., Worsnop, D.R., Chakrabarty, R.K., Moosmuller, H., Arnott, W.P., Schwarz, J.P., Gao, R.-S., Fahey, D.W., Kok, G.L., & Petzold, A. (2007). An inter-comparison of instruments measuring black carbon content of soot particles. *Aerosol Science and Technology*, *41*(3), 295–314.
Stevens, E., & Steeper, R. (2001). Piston wetting in an optical DISI engine: fuel films, poolfires, and soot generation. *SAE International Journal of Engines*, *110*, 1287–1294.
Storey, J.M., Barone, T., Norman, K., Lewis, S. (2010). Ethanol blend effects on direct injection spark-ignition gasoline vehicle particulate matter emissions, SAE Technical Paper, 2010-01-2129.
Storey, J.M., Lewis, S., Szybist, J., Thomas, J., Barone, T., Eibl, M., Nafziger, E., Kaul, B. (2014). Novel characterization of GDI engine exhaust for gasoline and mid-level gasoline-alcohol blends, SAE Technical Paper 2014-01-1606.
Szybist, J.P., Youngquist, A.D., Barone, T.L., Storey, J.M., Moore, W.R., Foster, M., & Confer, K. (2011). Ethanol blends and engine operating strategy effects on light-duty spark ignition engine particle emissions. *Energy and Fuels*, *25*, 4977–4985.
Turpin, B.J., & Lim, H. (2001). Species contributions to PM 2.5 mass concentrations: revisiting common assumptions for estimating organic mass. *Aerosol Science and Technology*, *35*(1), 602–610.
Twomey, S. (1977). The influence of pollution on the shortwave albedo of clouds. *Journal of thr Atmospheric Sciences*, *34*, 1146–1152.
Valavandidis, A., Fiotakis, K., & Vlachogianni, T. (2008). Airborne particulate matter and human health: toxicological assessment and importance of size and composition of particles for oxidative damage and carcinogenic mechanisms. *Journal of Environmental Science and Health, Part C*, *26*(4), 339–362.
Verma, V., Shafer, M.M., Schauer, J.J., & Sioutas, C. (2010). Contribution of transistion metals in the reactive oxygen species activity of PM emissions from retrofitted heavy-duty vehicles. *Atmospheric Environment*, *44*(39), 5165–5173.
Wang, S.C., & Flagan, R.C. (1990). Scanning electrical mobility spectrometer. *Aerosol Science and Technology*, *13*, 230–240.
Yang, W., Peters, J., & Williams, R. (2008). Inhaled nanoparticles–a current review. *International Journal of Pharmaceuticals*, *356*, 239–247.
Yung-Fang, Y.Y. (1980). Ocxdation of alkanes over noble metal catalysts. *Industrial and Engineering Chemistry Product Research and Development*, *19*, 293–298.
Zhao, F., Lai, M.C., & Harrington, D.L. (2006). Automotive spark-ignition direct-injection gasoline engines. *Progress in Energy and Combustion Science*, *25*(5), 437–562.